




# Laser induced periodic surface structures on polymer nanocomposites with carbon nanoadditives

René I. Rodríguez-Beltrán<sup>1,2</sup> · Sandra Paszkiewicz<sup>3</sup>  · Anna Szymczyk<sup>3</sup>  ·  
Zbigniew Roslaniec<sup>3</sup> · Aurora Nogales<sup>4</sup> · Tiberio A. Ezquerro<sup>4</sup> · Marta Castillejo<sup>2</sup> ·  
Pablo Moreno<sup>1</sup> · Esther Rebollar<sup>2</sup> 

Received: 30 June 2017 / Accepted: 6 October 2017 / Published online: 25 October 2017  
© Springer-Verlag GmbH Germany 2017

**Abstract** Laser induced periodic surface structures (LIPSS) are formed on poly(trimethylene terephthalate) and its composites with single-walled carbon nanotubes (SWCNT) and with both SWCNT and expanded graphite (EG) upon irradiation with a Q-Switched Nd:YAG laser (266 nm, 8 ns). The morphology of the polymer films was characterized by atomic force microscopy. A cantilever with a colloidal probe was used to obtain information about surface adhesion. Surface energies were estimated by contact angle measurements using different liquids. Chemical modification in the materials upon irradiation was assessed by Raman spectroscopy. Results show a dependence of the number of pulses required for LIPSS formation as a consequence of the presence of the carbon nanoadditive and an increase of the hydrophilic character of surfaces after irradiation. Moreover, the polar component of the surface free energy changes significantly and surface adhesion increases by the addition of the additive to the polymer matrix. Additionally, the adhesion force decreases after laser nanostructuring as a consequence of a lower contact area in the nanostructured material.

## 1 Introduction

Polymer-based nanocomposites reinforced with carbon nanofillers [1–3] display interesting properties such as optical transparency in the visible region [4], improved mechanical properties [5, 6], electrical [5, 7] and thermal [8] conductivities, and barrier impermeability to vapors and gases [9].

Single-walled carbon nanotubes (SWCNT) were discovered in 1991 [10] and since then, they have attracted much attention due to their exceptional mechanical [11], electrical and thermal properties [12] along with large aspect ratio, small diameter and low mass density [13]. SWCNT have a relative high cost in comparison to other carbon nanoadditives which limits widespread application of SWCNT-based composites. Therefore, hybrid nanocomposites containing both SWCNT and other less expensive additives, were recently developed [4, 14]. Expanded Graphite (EG) is the material derived from natural graphite [15], with a layered/planar structure, where the atoms are covalently bonded in a honeycomb lattice in each layer, while bonding is weak perpendicularly to the plane. Polymers reinforced with EG show an improvement of their physical properties [16–19].

Another way of providing a certain functionality to a material consists in surface patterning in the micro- and nanoscale. Common techniques for generating polymer structures at the nanoscale are typically based on soft lithography methods [20–22]. However, they require multiple-steps and the use of clean-room facilities, high vacuum or complex mask fabrication. An alternative is the use of laser-based techniques, and in particular, the formation of Laser Induced Periodic Surface Structures (LIPSS), which allows to obtain large processed surface areas in many types of materials [23–29]. The formation of LIPSS on polymer surfaces has been observed using lasers with pulse duration from nanoseconds (ns) to femtoseconds (fs) at wavelengths

---

✉ Esther Rebollar  
e.rebollar@csic.es

<sup>1</sup> Grupo de Aplicaciones del Láser y Fotónica (ALF-USAL), Universidad de Salamanca, Pl. de la Merced s/n, 37008 Salamanca, Spain  
<sup>2</sup> Instituto de Química Física Rocasolano (IQFR-CSIC), Serrano 119, 28006 Madrid, Spain  
<sup>3</sup> West Pomeranian University of Technology, Piastow Av. 19, 70310 Szczecin, Poland  
<sup>4</sup> Instituto de Estructura de la Materia (IEM-CSIC), Serrano 121, 28006 Madrid, Spain

from the ultraviolet (UV) to the infrared (IR) [27, 28, 30–32]. LIPSS formation upon irradiation with ns pulses requires the use of a linearly polarized laser at a wavelength efficiently absorbed by the polymer and fluences well below the ablation threshold [27, 30]. LIPSS are formed as the result of the interference between the incident and the surface-scattered waves, and a positive feedback process [27, 30, 33]. Upon irradiation, the material surface is heated and for LIPSS formation it is necessary to raise the temperature to overcome the glass transition temperature ( $T_g$ ) or the melting temperature ( $T_m$ ) for amorphous and semicrystalline polymers, respectively. LIPSS are aligned parallel to the polarization of the laser beam and their period ( $L$ ) is related to the laser wavelength ( $\lambda$ ) according to the expression  $L = \lambda / (n_e - \sin\theta)$ , where  $n_e$  is the effective refraction index of the material, and  $\theta$  is the angle of incidence [34].

In this work, we present a systematic study of the formation of LIPSS on poly(trimethylene terephthalate) (PTT) reinforced with SWCNT and a mixture of SWCNT and EG using UV ns pulses. Atomic force microscopy (AFM) has been performed to analyze the morphology of the LIPSS. Moreover, AFM employing a colloidal probe was used to characterize the adhesion of non-irradiated and irradiated samples. Contact angle (CA) characterization was achieved with different liquids to determine the surface free energy components in the polymer and the nanocomposite, before and after irradiation. Finally, Raman spectroscopy measurements were carried out to identify possible chemical modifications during LIPSS formation.

## 2 Experimental

Free-standing films of PTT reinforced with SWCNT and with SWCNT and EG were used. SWCNT properties (Grafen Chemical Industries, Ankara, Turkey) according to the supplier data are: diameter  $< 2$  nm, electrical conductivity  $> 100$  S/cm, length 5–30  $\mu\text{m}$ , purity  $> 95\%$ , surface area 380  $\text{m}^2/\text{g}$ . EG was provided by the Polymer Institute of Slovak Academy of Science with platelets size of around 50  $\mu\text{m}$ . Nanocomposites were prepared by in situ polymerization as described elsewhere [4, 35].

The SWCNT concentration was 0.3 wt%, while hybrid nanocomposites contain 0.1 wt% of EG and 0.1 wt% of SWCNT. PTT and its composites were melted at 255  $^\circ\text{C}$  and pressed for 2 min under 5 bar pressure and 2 min under 10 bar pressure. The obtained films have a thickness of approximately 0.4 mm and a roughness of  $2.9 \pm 0.1$ ,  $2.6 \pm 0.2$ , and  $8.0 \pm 0.5$  nm for PTT, PTT/SWCNT 0.3 wt% and PTT/EG 0.1 wt% + SWCNT 0.1 wt% respectively.

Wide angle X-ray scattering (WAXS) measurements were carried out using a Panalytical XPert PRO to determine the crystallinity of the samples after the preparation

process. The glass-transition and melting temperatures of the materials were measured by differential scanning calorimetry (DSC) by encapsulating them in aluminum pans. These calorimetric measurements were performed on a Perkin–Elmer DSC8500 instrument equipped with an Intracooler 2 subambient device and calibrated with high-purity indium standards. The heating rate was set to 10  $^\circ\text{C}/\text{min}$  in the temperature range 30–240  $^\circ\text{C}$ .

The films were irradiated using a linearly polarized laser beam from a Q-Switched Nd:YAG system (Lotis TII LS-2131M), at a wavelength of 266 nm, pulse duration of 8 ns and repetition rate of 10 Hz. Irradiation was performed in ambient air and at normal incidence.

Topography was analyzed by AFM using a Multimode 8 AFM equipped with a Nanoscope V controller (Bruker) in tapping mode with silicon probes (NSG30 by NT-MDT). AFM images were analyzed using the software Nanoscope Analysis 1.50 (Bruker). Adhesion measurements were performed by the colloidal probe technique using the same AFM equipment and the colloidal probe CPM-SiO<sub>2</sub>-A/Au by NT-MDT with a sphere size of 5–9  $\mu\text{m}$ .

For contact angle (CA) measurements, a pocket goniometer PG2 (FIBRO system) was used. The static wetting CA was measured at room temperature and ambient humidity using deionized water, paraffin oil and glycerol as liquid probes. The surface free energy components were calculated from the measured CA values.

Finally, Raman spectra were recorded using a micro-Raman spectrometer (Renishaw InVia 0310-02), with a laser excitation at 785 nm. The spectra were acquired with a spectral resolution of 2  $\text{cm}^{-1}$  using a 50 $\times$  objective to a spot with a diameter  $< 1$   $\mu\text{m}$  on the samples. Laser power conditions were those that ensured the integrity of the polymer.

## 3 Results and discussion

As revealed by WAXS experiments (Fig. 1a), PTT films were clearly amorphous, while the composites exhibited traces of crystallinity that should be ascribed to the presence of the additives.

Figure 1b shows the DSC traces for PTT and its composites. No differences in  $T_g$  and  $T_m$  are observed for the nanocomposites when compared to the raw polymer. The values of  $T_g$  and  $T_m$  are 52 and 227  $^\circ\text{C}$ , respectively, for all samples. The main effect can be observed in the cooling traces. Carbon additives in both cases act as nucleating agents provoking crystallization at higher temperatures upon cooling from the melt in comparison to the neat polymer matrix.

LIPSS were obtained for films of both PTT and its nanocomposites. Figure 2 displays AFM topography images of PTT (upper row), PTT/SWCNT 0.3 wt% (middle row) and PTT/EG 0.1 wt% + SWCNT 0.1 wt% (bottom row) samples

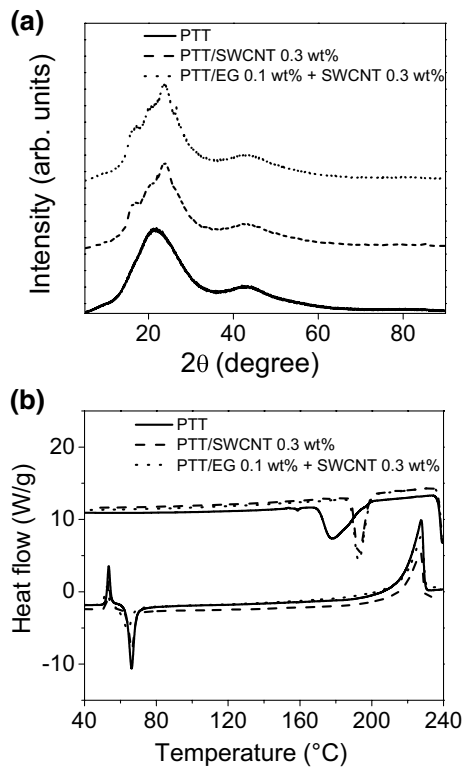
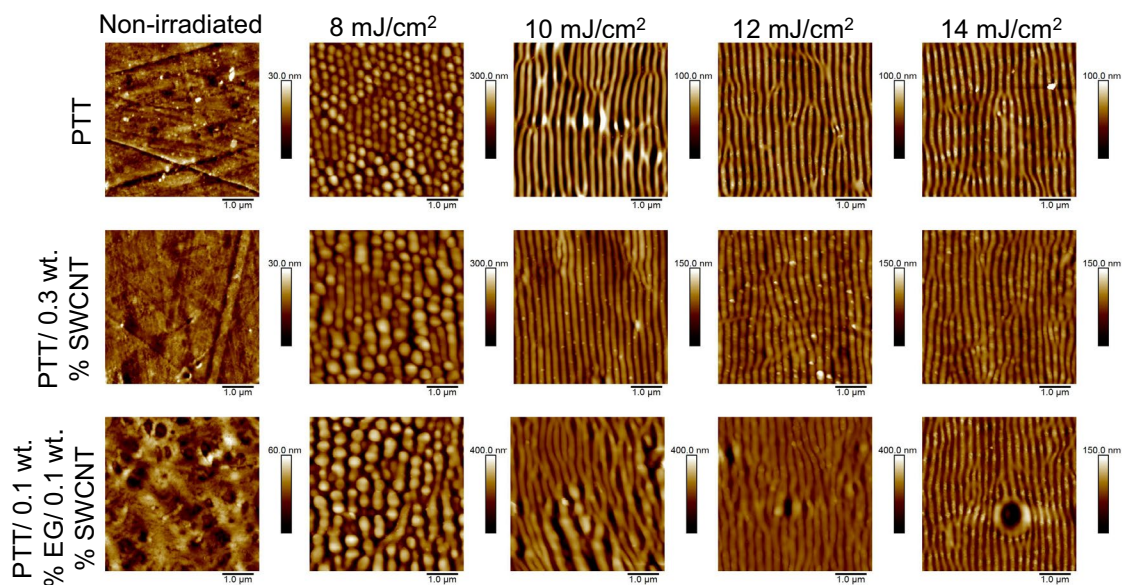


**Fig. 1** **a** Wide angle X-ray scattering patterns and **b** differential scanning calorimetry traces of PTT and PTT based nanocomposites with SWCNT 0.3 wt% and with EG 0.1 wt% + SWCNT 0.1 wt% as labelled

before irradiation, and the evolution on the formation of the nanostructures generated by laser irradiation with different fluences at 3000 pulses. In all cases, ripples obtained have a period close to the irradiation wavelength and they are parallel to the polarization of the laser beam.

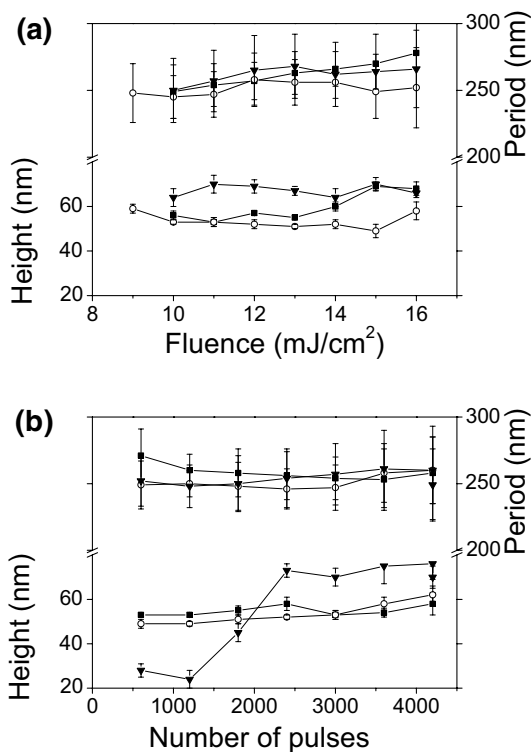
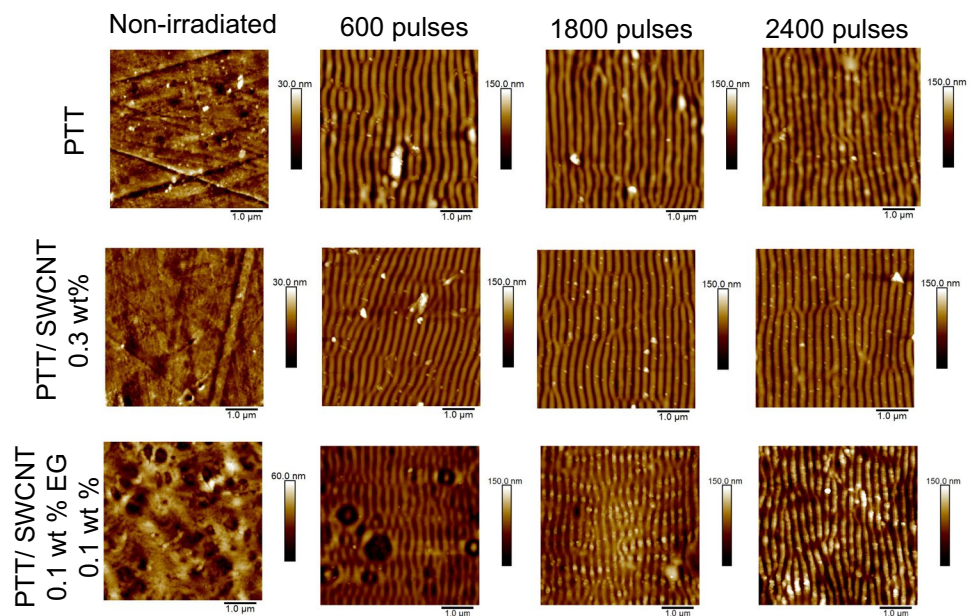
Additionally, LIPSS formation was studied in the different materials as a function of the number of pulses for a constant fluence of  $11 \text{ mJ/cm}^2$ , as shown in Fig. 3.

Figure 4 shows the dependence of the period and height of the obtained LIPSS as a function of the laser fluence (Fig. 4a) and of the number of pulses (Fig. 4b). In the case of the dependence on the fluence, there are no significant differences for the periods and heights obtained for the different samples. The period is close to the irradiation wavelength and the height of the LIPSS reaches values up to 70 nm. However, a significant difference is observed in the study of the formation of the ripples as a function of the number of pulses. In particular, LIPSS formation on PTT/SWCNT 0.1 wt%+EG 0.1 wt% seems to be slower and the number of pulses needed to reach a height similar to the one reached for PTT and PTT/SWCNT 0.3 wt% is higher. It is important to note that the LIPSS generated upon irradiation with nanosecond pulses requires the heating of the surface material above  $T_g$ , to allow the polymer chains to rearrange, and repetitive irradiation to facilitate the feedback mechanism [27, 33]. To explain the differences observed for the number of pulses needed for LIPSS formation, we have to consider the differences in thermal properties of the films as a consequence of the presence of the nanoadditives. A



**Fig. 2** AFM topography images of the surface of PTT (upper row), PTT/SWCNT 0.3 wt% (middle row) and PTT/EG 0.1 wt% + SWCNT 0.1 wt% (bottom row) films irradiated at 266 nm with 3000 pulses at the indicated fluences

**Fig. 3** AFM topography images of the surface of PTT (upper row), PTT/SWCNT 0.3 wt% (middle row) and PTT/EG 0.1 wt% + 0.1 SWCNT wt% (bottom row) films irradiated at 266 nm with a fluence of 11 mJ/cm<sup>2</sup> at the indicated number of pulses



**Fig. 4** Height and period of PTT (filled square), PTT/SWCNT 0.3 wt% (open circle) and PTT/EG 0.1 wt% + 0.1 SWCNT wt% (inverted filled triangle) as a function of **a** fluence at a constant number of pulses of 3000 and **b** number of pulses at a constant fluence of 11 mJ/cm<sup>2</sup>

combination of carbon nanofillers with different dimensionality (1D and 2D) can exert a synergic effect on the physical properties and in particular, on the thermal conductivity.

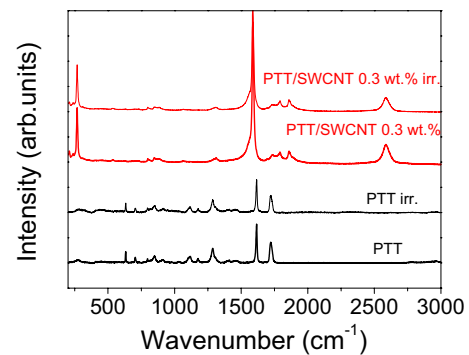


**Fig. 5** Raman spectra for non-irradiated and irradiated PTT and PTT/SWCNT 0.3 wt% films. Spectra have been vertically shifted for clarity

It has been reported that thermal conductivity increases in several polymer materials reinforced with 1D (CNT) and 2D [EG, graphite nanoplatelets (GNP)] [14, 36]. An increase in the thermal conductivity would affect the formation of ripples in the composite surfaces. The temperature reached at the surface upon irradiation will be lower for higher thermal conductivity, and thus as observed, a higher number of pulses will be needed for the feedback mechanism to effectively contribute to LIPSS formation [37].

Figure 5 shows the Raman spectra corresponding to PTT and PTT/SWCNT 0.3 wt% before and after irradiation. In the case of PTT, bands assigned to the polymer are observed [38, 39]. In the Raman spectra of the reinforced PTT, the band assigned to the graphitic *G* and *G'* bands are observed at around 1580 and 2600 cm<sup>-1</sup>, respectively [40]. The *D* band, located at 1350 cm<sup>-1</sup> is not clearly detected as it overlaps with bands ascribed to the polymer matrix.



Nevertheless, the low intensity of the *D* band in comparison to that of the *G* band indicates that SWCNT are of high purity. In addition to these bands, the radial breathing modes are observed in the region of 200–300  $\text{cm}^{-1}$ . These modes correspond to the coherent vibration of the carbon atoms in the radial direction and depend on the diameter of the nanotubes [41, 42] and on the nanotubes aggregation [43, 44]. The Raman spectra of the irradiated and the non-irradiated samples are very similar, indicating that no significant changes are induced upon laser irradiation in contrast with what has been reported previously [45]. This could be explained taking into account that the height of the nanostructures is below 100 nm while the penetration depth of the Raman excitation is around 700 nm. Therefore, the technique has not enough resolution to distinguish any change taking place at the nanostructures scale.

To further analyze the physico-chemical surface modifications induced by laser irradiation, CAs of water, glycerol and paraffin oil were measured. As an example, Fig. 6 shows water, glycerol and paraffin oil droplets on non-irradiated and irradiated PTT/SWCNT 0.3 wt% surfaces. The results for non-irradiated and irradiated samples for each liquid probe are listed in Table 1.

All the non-irradiated samples are slightly hydrophilic and there are no significant differences for the films of pure polymer and polymer with nanoadditives. For the irradiated samples, the water CA decreases indicating that the

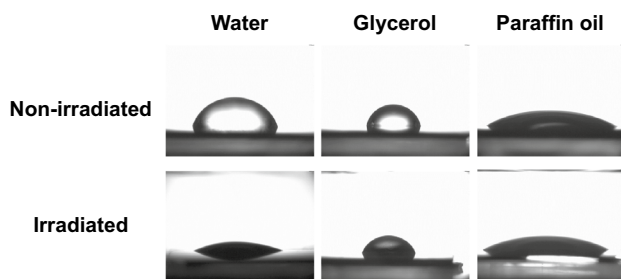


**Fig. 6** Images of a drop of different liquids on top of the surface of PTT/SWCNT 0.3 wt% non-irradiated and irradiated at 11  $\text{mJ}/\text{cm}^2$  and 3000 pulses

**Table 1** CA values of water, glycerol and paraffin oil for non-irradiated and irradiated PTT, PTT/SWCNT 0.3 wt%, and PTT/EG 0.1 wt% + SWCNT 0.1 wt% samples measured 24 h after irradiation, and surface free energy components ( $\text{mJ}/\text{m}^2$ ) calculated using the OWRK-model [46]

Sample	Contact angle			Surface free energy		
	Water	Glycerol	Paraffin oil	$\gamma_s^d$	$\gamma_s^p$	$\gamma_s^{\text{TOT}}$
PTT, non-irradiated	$72 \pm 3$	$70 \pm 4$	$28 \pm 4$	23.5	10.7	34.2
PTT, irradiated	$27 \pm 2$	$69 \pm 4$	$25 \pm 3$	17.8	35.2	53.0
PTT/SWCNT 0.3 wt%, non-irradiated	$72 \pm 4$	$66 \pm 3$	$29 \pm 2$	24.2	11.1	35.3
PTT/SWCNT 0.3 wt%, irradiated	$24 \pm 3$	$67 \pm 4$	$22 \pm 2$	18.4	36.2	54.6
PTT/EG 0.1 wt%/SWCNT 0.1 wt%, non-irradiated	$77 \pm 3$	$73 \pm 3$	$27 \pm 3$	24.0	8.1	32.1
PTT/EG 0.1 wt%/SWCNT 0.1 wt%, irradiated	$25 \pm 3$	$74 \pm 3$	$24 \pm 2$	16.8	35.4	52.2

materials become more hydrophilic after irradiation. This is in agreement with previous results in similar materials and can be explained by a slight surface oxidation taking place upon irradiation in air [45]. In the case of the CA of glycerol and paraffin oil, no significant changes are observed after irradiation.

The CA is related with the surface free energy components between the liquid (l) and the first monolayer of the tested solid (s). To estimate the surface free energy components, the Owens, Wendt, Rabel and Kaelble model (OWRK-model) was applied [46]. This model uses the Young's equation to determine the surface total energy  $\gamma_s^{\text{TOT}}$  and the dispersive  $\gamma_s^d$  and polar components  $\gamma_s^p$  of the surface tension. At least two liquids with known dispersive and polar components of the surface tension are required to determine the surface free energy of the solid, wherein at least one of the liquids must have a polar component  $> 0$ . We have used water and glycerol as polar liquids and paraffin oil as apolar one [45]. The calculated values are summarized in Table 1. There are no significant differences between the values obtained for the different samples. In all the cases, comparing the values obtained for the non-irradiated and the irradiated samples, the dispersive component is slightly smaller for the latter, while the polar component of the surface tension clearly increases upon irradiation. This could suggest that new functional groups in the outer part of the tested solid have been formed. Thus, the increment in the polarity and the hydrophilicity of the nanostructured samples can be explained on the basis of the formation of hydrophilic groups that combined with the oxygen from air, introduce carbonyl, hydroxyl and carboxyl polar groups. The surface total energy also increases after irradiation. Additional analysis was carried out 96 h after irradiation and surface free energy remains constant in time.

Finally, measurements of adhesion forces were performed using AFM with a colloidal tip. Figure 7a shows the force curves corresponding to a PTT nanostructured sample. From the retracting curve, the adhesion force value can be estimated, which corresponds to the difference between the baseline and the minimum force. The results of the analysis are displayed in Fig. 7b. Before irradiation, the adhesion

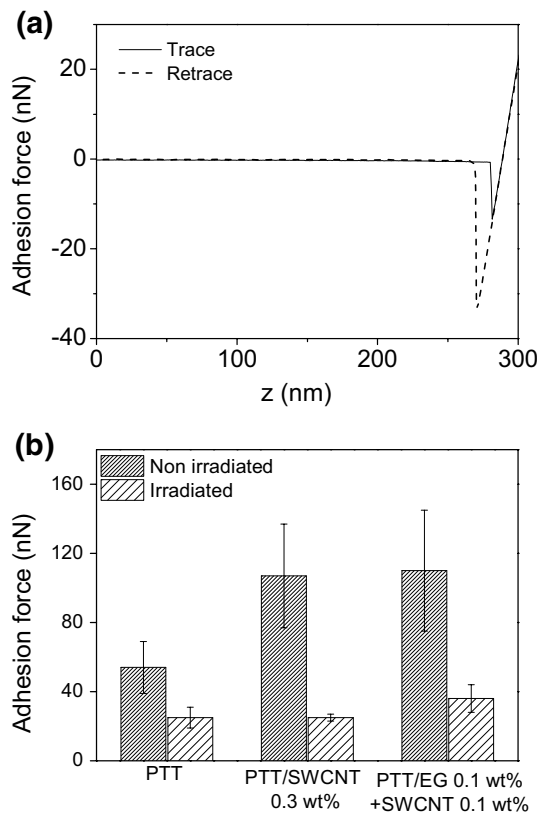


**Fig. 7** **a** Adhesion force versus distance for nanostructured PTT, **b** adhesion force as determined by the colloidal probe technique for PTT, PTT/SWCNT 0.3 wt% and PTT/EG 0.1 wt% + SWCNT 0.1 wt%

force in the composites is higher than the value obtained for the pure polymer sample. After irradiation, the adhesion force decreases in all the cases. This decrease can be explained considering the decrease in the effective contact area under the colloidal probe for the samples with LIPSS. Apparently, this cannot be compensated by the enhanced adhesion expected from the increase in the surface polarity. This effect has been previously observed in other micro- and nanopatterned polymer surfaces [47–49].

#### 4 Conclusions

Laser induced periodic surface structures were obtained on PTT and PTT reinforced with SWCNT and SWCNT and EG. In all cases ripples with a period close to the laser irradiation wavelength were obtained, although differences in the number of pulses needed to obtain LIPSS in each case are observed. These differences may be explained by the thermal conductivity modification resulting from the addition of carbon fillers. In particular, higher values of thermal conductivity imply lower temperatures reached upon

irradiation with every single pulse and a less effective LIPSS formation process. After laser irradiation, samples become more hydrophilic and the surface free energy and its polar component increase for all the samples tested. This is related to chemical modifications on the material surface upon laser irradiation. Additionally, adhesion force decreases for the films with LIPSS as a consequence of a smaller contact area in the nanostructured materials.

**Acknowledgements** The authors gratefully acknowledge financial support from the MINECO (FIS2013-44174-P, MAT2014-59187-R, MAT2015-66443-C02-1-R, FIS2015-71933-REDT, CTQ2016-75880-P) and Junta de Castilla y León (Project SA046U16). RIR is grateful for the International Scholarship number 314197 provided by Consejo Nacional de Ciencia y Tecnología (CONACyT-México) and E.R. thanks MINECO for a Ramón y Cajal contract (RYC-2011-08069). The authors thank J. V. García Ramos for the Raman measurements.

#### References

1. S. Stankovich, D.A. Dikin, G.H.B. Dommett, K.M. Kohlhaas, E.J. Zimney, E.A. Stach, R.D. Piner, S.T. Nguyen, R.S. Ruoff, *Nature* **442**, 282 (2006)
2. P.-C. Ma, N.A. Siddiqui, G. Marom, J.-K. Kim, *Compos. Part A: Appl. Sci. Manuf.* **41**, 1345 (2010)
3. R. Sengupta, M. Bhattacharya, S. Bandyopadhyay, A.K. Bhowmick, *Prog. Polym. Sci.* **36**, 638 (2011)
4. S. Paszkiewicz, A. Szymczyk, X.M. Sui, H.D. Wagner, A. Linares, A. Cirera, A. Varea, T.A. Ezquerro, Z. Roslaniec, *J. Appl. Polym. Sci.* **134**, 44370 (2017)
5. A. Ammar, A.M. Al-Enizi, M.A. AlMaadeed, A. Karim, *Arabian J. Chem.* **9**, 274 (2016)
6. S.H. Park, P.R. Bandaru, *Polymer* **51**, 5071 (2010)
7. A. Linares, J.C. Canalda, M.E. Cagiao, M.C. García-Gutiérrez, A. Nogales, I. Martín-Gullón, J. Vera, T.A. Ezquerro, *Macromolecules* **41**, 7090 (2008)
8. Z. Tao, H. Wang, X. Li, Z. Liu, Q. Guo, *J. Appl. Polym. Sci.* **134**, 44843 (2017)
9. H.-D. Huang, P.-G. Ren, J. Chen, W.-Q. Zhang, X. Ji, Z.-M. Li, *J. Membr. Sci.* **409–410**, 156 (2012)
10. S. Iijima, *Nature* **354**, 56 (1991)
11. J.P. Lu, *Phys. Rev. Lett.* **79**, 1297 (1997)
12. M. Monthieux, *Carbon* **40**, 1809 (2002)
13. G. Guanghua, Ç. Tahir, A.G. William, III, *Nanotechnology* **9**, 184 (1998)
14. S. Paszkiewicz, A. Szymczyk, X.M. Sui, H.D. Wagner, A. Linares, T.A. Ezquerro, Z. Roslaniec, *Compos. Sci. Technol.* **118**, 72 (2015)
15. A. Celzard, J.F. Maréché, G. Furdin, *Prog. Mater. Sci.* **50**, 93 (2005)
16. W. Zheng, S.-C. Wong, *Compos. Sci. Technol.* **63**, 225 (2003)
17. M. Zhang, D.-J. Li, D.-F. Wu, C.-H. Yan, P. Lu, G.-M. Qiu, *J. Appl. Polym. Sci.* **108**, 1482 (2008)
18. R.K. Goyal, P.A. Jagadale, U.P. Mulik, *J. Appl. Polym. Sci.* **111**, 2071 (2009)
19. S. Paszkiewicz, A. Szymczyk, Z. Špitalský, M. Soccio, J. Mosnáček, T.A. Ezquerro, Z. Roslaniec, *J. Polym. Sci. Part B: Polym. Phys.* **50**, 1645 (2012)

20. H. Schiff, J. Vac. Sci. Technol. B Microelectron. Nanometer. Struct. Process. Meas. Phenom. **26**, 458 (2008)
21. D. Qin, Y. Xia, G.M. Whitesides, Nat. Protoc. **5**, 491 (2010)
22. J.P. Rolland, E.C. Hagberg, G.M. Denison, K.R. Carter, J.M. De Simone, Angew. Chem. Int. Ed. **43**, 5796 (2004)
23. M. Sanz, E. Rebollar, R.A. Ganeev, M. Castillejo, Appl. Surf. Sci. **278**, 325 (2013)
24. J. Bonse, S. Höhm, S.V. Kirner, A. Rosenfeld, J. Krüger, IEEE J. Sel. Topics Quantum. Electron. **23**, 1 (2017)
25. P. Gregorčič, M. Sedlaček, B. Podgornik, J. Reif, Appl. Surf. Sci. **387**, 698 (2016)
26. A. Talbi, A. Petit, A. Melhem, A. Stolz, C. Boulmer-Leborgne, G. Gautier, T. Defforge, N. Semmar, Appl. Surf. Sci. **374**, 31 (2016)
27. E. Rebollar, M. Castillejo, T.A. Ezquerra, Eur. Polym. J. **73**, 162 (2015)
28. S. Pérez, E. Rebollar, M. Oujja, M. Martín, M. Castillejo, Appl. Phys. A **110**, 683 (2013)
29. P. Slepíčka, O. Neděla, N. Slepíčková Kasálková, P. Sajdl, V. Švorčík, Int. J. Nanotechnol. **14**, 399 (2017)
30. E. Rebollar, S. Pérez, J.J. Hernández, I. Martín-Fabiani, D.R. Rueda, T.A. Ezquerra, M. Castillejo, Langmuir **27**, 5596 (2011)
31. E. Rebollar, J.R.V.d.. Aldana, J.A. Pérez-Hernández, T.A. Ezquerra, P. Moreno, M. Castillejo, Appl. Phys. Lett. **100**, 041106 (2012)
32. M. Forster, W. Kautek, N. Faure, E. Audouard, R. Stoian, Phys. Chem. Chem. Phys. **13**, 4155 (2011)
33. E. Rebollar, D.R. Rueda, I. Martín-Fabiani, Á. Rodríguez-Rodríguez, M.-C. García-Gutiérrez, G. Portale, M. Castillejo, T.A. Ezquerra, Langmuir **31**, 3973 (2015)
34. D.W. Bäuerle, *Laser Processing and Chemistry* (Springer-Verlag, Berlin Heidelberg, 2011)
35. S. Paszkiewicz, I. Pawelec, A. Szymczyk, Z. Roslaniec, Polimery/ Polymers **61**, 172 (2016)
36. S. Kumar, L.L. Sun, S. Caceres, B. Li, W. Wood, A. Perugini, R.G. Maguire, W.H. Zhong, Nanotechnology. **21**, 105702 (2010)
37. J. Cui, A. Nogales, T.A. Ezquerra, E. Rebollar, Appl. Surf. Sci. **394**, 125 (2017)
38. F.J. Boerio, S.K. Bahl, G.E. McGraw, J. Polym. Sci. Polym. Phys. Edit. **14**, 1029 (1976)
39. I.M. Ward, M.A. Wilding, Polymer **18**, 327 (1977)
40. A.G. Souza Filho, A. Jorio, A.K. Swan, M.S. Ünlü, B.B. Goldberg, R. Saito, J.H. Hafner, C.M. Lieber, M.A. Pimenta, G. Dresselhaus, M.S. Dresselhaus, Phys. Rev. B. **65**, 085417 (2002)
41. M. Lucas, R.J. Young, Phys. Rev. B. **69**, 085405 (2004)
42. U.D. Venkateswaran, D.L. Masica, G.U. Sumanasekera, C.A. Furtado, U.J. Kim, P.C. Eklund, Phys. Rev. B. **68**, 241406 (2003)
43. D.A. Heller, P.W. Barone, J.P. Swanson, R.M. Mayrhofer, M.S. Strano, J Phys Chem B. **108**, 6905 (2004)
44. M.C. García-Gutiérrez, A. Nogales, D.R. Rueda, C. Domingo, J.V. García-Ramos, G. Broza, Z. Roslaniec, K. Schulte, R.J. Davies, T.A. Ezquerra, Polymer **47**, 341 (2006)
45. E. Rebollar, S. Pérez, M. Hernández, C. Domingo, M. Martín, T.A. Ezquerra, J.P. García-Ruiz, M. Castillejo, Phys. Chem. Chem. Phys. **16**, 17551 (2014)
46. D.K. Owens, R.C. Wendt, J. Appl. Polym. Sci. **13**, 1741 (1969)
47. B. Bharat, J. Yong Chae, J. Phys. Condens. Matter. **20**, 225010 (2008)
48. E. Wohlfart, J.P. Fernández-Blázquez, E. Knoche, A. Bello, E. Pérez, E. Arzt, A. del Campo, Macromolecules. **43**, 9908 (2010)
49. Z. Burton, B. Bhushan, Nano Lett. **5**, 1607 (2005)